P18 CCS: Seismic Risk Evaluation

Report for TAQA Energy BV

Fenix Consulting Delft BV
C.J. de Pater

Date
November 2019

P18 CCS: Seismic Risk Evaluation

Report for TAQA Energy BV

Date
November 2019

DISCLAIMER

Fenix Consulting Delft nor any person acting on behalf of Fenix:

- **Makes any warranty or representation, express or implied, with respect to the accuracy, completeness, or usefulness of the information contained in this report, or that the use of any apparatus, method, or process disclosed in this report may not infringe privately owned rights; or**

- **Assumes any liability with respect to the use of, or for damages resulting from the use of, any information, apparatus, method, or process disclosed in this report.**

Executive Summary

TAQA is planning (with PORTHOS partners) to use the depleted P18 fields for CO2 storage. The location of the fields is just offshore Hoek van Holland.
The various compartments are distinguished as several fields: the P18-2 field (consisting of several compartments), while the P18-4 and P18-6 fields consist of a single compartment. The P18-2 field is isolated from the P18-4 field, which has a much shallower GWC.
Seismicity is mainly a concern because it may lead to upward migration of CO2 if fault slippage enhances conductivity of the faults. Since the fields are more than 5km from the shoreline, there are no vulnerable surface structures that might be damaged by earthquakes.
In gas fields, the main source of seismicity is differential compaction that causes stress concentrations on the faults. As yet, the reservoirs have been strongly depleted but no recorded seismicity was induced. Upon injection, the reservoir pressure will be restored so that stability of the faults is improved. Other mechanisms of seismicity could be local pressure changes during CO2 injection and cooling of the reservoir due to injected gas expansion into the low-pressure reservoir.
The excess pressure will be very low, so this is unlikely to induce seismicity. However, extensive cooling will reduce the stress because of reservoir shrinkage. Some injectors are only a few hundred meters from a fault, so the cold front could reach the fault after several years. Fortunately, the thermal stress effect is similar to the differential compaction effect, although thermal stress reduces confining stress on the fault while differential compaction mainly increases shear stress. However, the slippage condition is equivalent and therefore the probability of seismicity by thermal stress reduction is deemed low since no seismicity was observed during compaction of the fields. Although, the CO2 injection carries a potential hazard of induced seismicity, it follows from the analysis that the probability of seismicity is low and therefore risk is negligible.
Compared with analogous CO2 injection projects like Sleipner (North Sea), In Salah (Algeria) or Weyburn (Canada), the P18 project falls in a class of low probability of seismicity. In the In Salah project, some weak seismicity was induced (of magnitude 1.7) but this is a low-permeability aquifer that had significant pressure increase. In the Sleipner project, CO2 is injected into a huge high-permeability aquifer, which ensures that pressure changes are small. This is similar to injection into a depleted gas field like P18, where the excess injection pressure changes are also small so that geomechanical effects are small.

Conclusions

- The P18 fields have been almost depleted and the reservoir properties also indicate that compaction induced seismicity might be possible. However, no seismicity has been observed, so that maximum magnitude of any seismicity should be less than 1.5.
- Since pressure will be restored during CO2 injection and no seismicity was induced during depletion, the risk of seismicity during injection is deemed negligible (Teatini *et al.*, 2019).
- Since no seismicity has been observed, the fields fall in the class of negligible risk, so that only monitoring with the regional network is required.
- Fracture propagation during injection is unlikely, but due to thermal stress reduction a fracture could be propagated from the injector, if the modulus or thermal expansion coefficient is higher than expected.
    - An injection fracture will be confined to the cooled zone and it will also propagate along the major faults, in view of the stress orientation. Therefore, hitting a fault or breaching the overburden or underburden is very unlikely.
- Local pressure increase by injection is quite small, so that geomechanical effects of pressure will be negligible. The restoration of pressure will be up to virgin pressure so that stability of the faults is actually improved. In this sense, the P18 field falls in the low-risk category of worldwide CO2 storage projects, analogous to the Sleipner storage project in the Norwegian sector of the North Sea.

Contents

EXECUTIVE SUMMARY ..... **III**

Contents iv

List of Figures v

List of Tables vi

Nomenclature vii

1 INTRODUCTION **1**

2 MECHANISMS OF SEISMICITY **4**

3 RESERVOIR PROPERTIES, PRESSURE AND FAULT SYSTEM **6**

Fault System 8

4 STRESS ANALYSIS **14**

5 FRACTURE SIMULATIONS **16**

6 RISK ANALYSIS **18**

Injection Seismicity Risk Analysis 22

Risk Classification 25

Discussion 26

REFERENCES **26**

List of Figures

Figure 1: Overview of the locations of P18 and nearby P15 fields (After TAQA, 2009). 1

Figure 2: Overview of the three P18 fields (P18-2, P18-4, and P18-6), and the blocks of the P18-2 Field (2-I, 2-II, 2-III, and 2-IV). Red line indicates the position of the cross section shown in Figure 4 (TNO, 2019). 1

Figure 3: Lithology of the Triassic P18-2 field and overburden. The Hardegsen (Top Bunter) and Detfurth layers comprise the reservoir with a small contribution from the tight Volpriehausen layer (TNO, 2019). 2

Figure 4: Cross section through the P18-2 field, showing block 2-I with initial water saturation. The location of the cross section is shown in Figure 2 (TNO, 2019). 2

Figure 5: Correlation between size of rupture area (for a square area) and earthquake magnitude. Using seismic traces the size of the slip area and the stress drop can be inferred. These slip area dimensions are plotted for depletion earthquakes in Bergermeer and Groningen. For a computed maximum slip area, the empirical relation gives a conservative estimate of magnitude. The TNO correlation is based on a theoretical relation and is more conservative. 4

Figure 6: Map of gas fields in the Netherlands. Induced earthquakes in the Netherlands are concentrated in two areas: one near the Groningen gas field and another near the Bergermeer field and neighbouring fields that lie on the same trend. The P18 fields belong to a trend of gas fields, extending from Zuid-Holland to offshore P18 and P15 blocks (West-Netherlands Basin) that are seismically quiet. 5

Figure 7: Logs and lithology in well P18-04A2. DSI readings from log displays were used to compute the modulus in overburden and reservoir. The Hardegsen reservoir has lower modulus than the overburden. 6

Figure 8: Stress gradients derived from P18-1 logs and LOT pressures as well as fracture gradients determined in nearby P15 and P12 fracture injection PFO's. The logs in the P18-2 well yielded the same result for the reservoir stress. 7

Figure 9: Stress orientation in the North Sea area near P18 (World Stress Map, 2016). 8

Figure 10: Faults in the P18-2 field, with well P18-2-A5. The dashed line indicates the cross-section along the minimum stress direction. 9

Figure 11: Faults in a cross-section through well P18-2-A5 along the minimum stress direction. The red ellipse indicates the injection interval. 9

Figure 12: Faults in the P18-2 field, with well P18-2-A1. The dashed line indicates the cross-section along the maximum stress direction. 10

Figure 13: Faults in a cross-section through well P18-2A1 along the minimum stress direction. The red ellipse indicates the injector. 10

Figure 14: Faults in a cross-section through well P18-2A1 along the maximum stress direction. The red ellipse indicates the injector. 10

Figure 15: Faults in the P18-2 field, with well P18-2A3. The dashed line indicates the cross-section along the minimum stress direction. 11

Figure 16: Faults in a cross-section through well P18-2A3 along the minimum stress direction. The red ellipse indicates the injector. 11

Figure 17: Faults in a cross-section through well P18-2A3 along the maximum stress direction. The red ellipse indicates the injector. 11

Figure 18: Faults in the P18-4 field, with well P18-4A2. The dashed line indicates the cross-section along the minimum stress direction. 12

Figure 19: Faults in the P18-4 field, in a cross-section through well P18-4A2 along the minimum stress direction. The red ellipse indicates the Injection interval in well. 12

Figure 20: Faults in the P18-6 field, with well P18-6A7ST1. The dashed line indicates the cross-section along the minimum stress direction. 13

Figure 21: Faults in a cross-section through well P18-6A7ST1 along the minimum stress direction. The red ellipse indicates the injector. 13

Figure 22: Critical excess pressure above reservoir pressure that is needed to destabilize a fault in the virgin state. 14

Figure 23: Critical excess pressure above reservoir pressure that is needed to destabilize a fault, after depletion. 14

Figure 24: Mohr Coulomb plot for stresses after depletion in the P18-2 reservoir. For a critically oriented fault, instability could occur with an excess pressure of 5.3MPa in the fault 15

Figure 25: Mohr Coulomb plot for virgin stresses in the P18-2 reservoir. Also, the effect of depletion and cooling by CO2 injection is plotted. 15

Figure 26: Pressure in base case fracture simulation for CO2 injection into P18-2 field. Since the pressure is much lower than the stress, no fracture propagation is possible. Only if the thermal stress would fall below the BHP a fracture could propagate. 16

Figure 27: Pressure in fracture simulation for CO2 injection into P18-2 field for higher modulus of 30GPa. Since thermal stress is proportional to the modulus, the lower stress facilitates fracturing after a few months injection. 17

Figure 28: pressure and temperature fronts in the simulation with fracturing. In agreement with detailed CO2 simulations, the cold front extends over several hundred meters after 5 years and after 1 year the extent is some 50 m which facilitates an 80 m fracture length. 17

Figure 29: Fracture size vs. time, for simulation with high modulus of 30GPa. 17

Figure 30: Risk map with surface risk index on the horizontal axis and subsurface risk index on the vertical axis. 18

Figure 31: Risk map for injection seismicity with surface risk index on the horizontal axis and subsurface risk index on the vertical axis. 24

Figure 32: Decision flow diagram for Seismic Risk Classification proposed by SoDM. There has been no past seismicity in P18 and the risk matrices for compaction as well as injection risk yield risk class I of negligible risk, monitoring with the regional network is sufficient. 25

List of Tables

Table 1: Average reservoir properties. Most properties apply to all three fields, but the pressure and stress changes apply to P18-2. The pressure for the other fields is listed in Table 3. 6

Table 2: Average properties of the reservoir layers. 7

Table 3: Reservoir pressures per field. 7

Table 4: Distance of injectors to nearby faults, within 1km distance. Distances were calculated from the centre of the Hardegsen interval. Yellow colour indicates boundary faults that have become stressed by differential compaction during depletion. 8

Table 5: Modulus from DSI log in P18-4 well, with E-factor. 19

Table 6: Total fault length and block volume for P18-2, P18-4 and P18-6 fields with the corresponding B-factor. The B-factor was also computed including only the boundary faults, which are most significant, but that yielded also a high value. 19

Table 7: Fault length and maximum magnitude of earthquakes that could be sustained by each fault. 19

Table 8: Reservoir bulk volumes and maximum magnitude that could be induced based on the compaction energy release. For P18-2 and P18-4 the volume change was computed assuming uniform pressure at full depletion. For P18-6 the volume change was computed with the simulated pressure at full depletion. Since most of the bulk volume of P18-6 experiences no pressure decrease, the volume change is relatively small. 19

Table 9: Subsurface risk factors for seismicity 20

Table 10: Surface risk factors. The factor for industrial installations was assigned 2, to allow for more platforms or other structures although at the moment no other platforms exist within 5km of the P18 field. 21

Table 11: Subsurface risk factors for injection seismicity. The weight factor recognizes the large significance of reservoir type for overall risk. 24

Nomenclature

Units: SI (m= metre, s= second, kPa =10^3Pa, MPa =10^6Pa, GPa =10^9Pa)

Dimensions: m= mass, L= length, t= time

Variable		Description	Units	Dimensions
A_p	:	Poroelastic coefficient	[-]	(-)
c	:	cohesion	[MPa]	(m/Lt^2)
E	:	Young's modulus	[GPa]	(m/Lt^2)
g	:	Stress gradient	[kPa/m]	(m/L^{2}t^2)
K_h	:	horizontal stress ratio	[-]	(-)
M_0	:	seismic moment	[N m]	(mL^2/t^2)
M	:	moment magnitude	[-]	(-)
p	:	pressure	[MPa]	(m/Lt^2)
V_{res}	:	reservoir volume	[m^3]	(L^3)
R_{crit}	:	Stress ratio: shear stress over effective normal stress	[-]	(-)
α_B	:	Biot coefficient	[-]	(-)
ν	:	Poisson's ratio	[-]	(-)
μ	:	friction coefficient	[-]	(-)
$\sigma_{H,max}$	:	maximum horizontal stress	[MPa]	(m/Lt^2)
$\sigma_{h,min}$	:	minimum horizontal stress	[MPa]	(m/Lt^2)
σ_{vert}	:	vertical stress	[MPa]	(m/Lt^2)
σ_n	:	normal stress on fault plane	[MPa]	(m/Lt^2)
τ	:	shear stress	[MPa]	(m/Lt^2)

1 Introduction

TAQA is planning (with PORTHOS partners) to use the depleted P18 fields for CO2 storage. The location of the fields and nearby fields are shown below in Figure 1.
The fields are indicated in the map of Figure 2. The P18-2 field consists of several compartments, while the P18-4 and P18-6 fields consist of a single compartment. The P18-2 field is isolated from the P18-4 field, which has a shallower GWC.

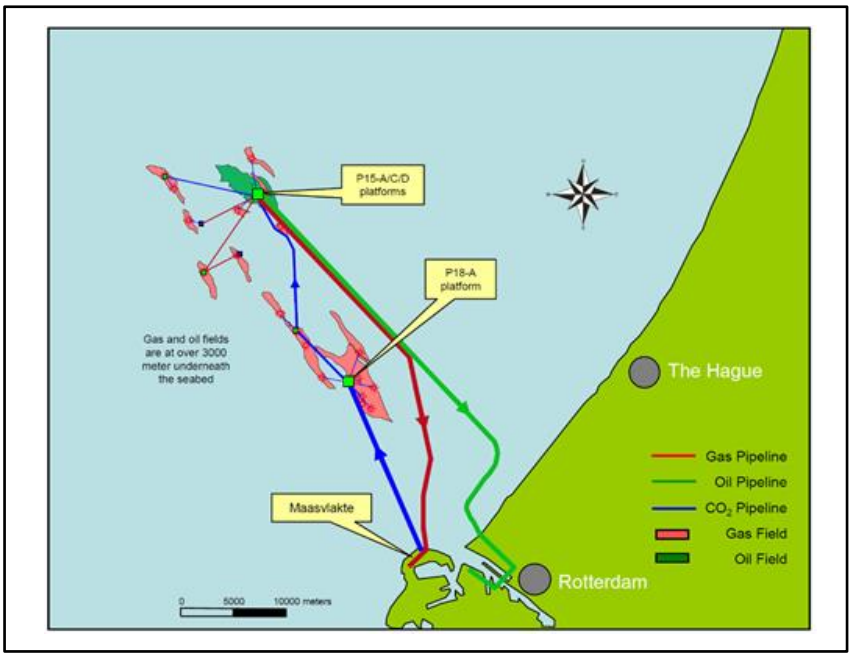

Figure 1: Overview of the locations of P18 and nearby P15 fields (After TAQA, 2009).

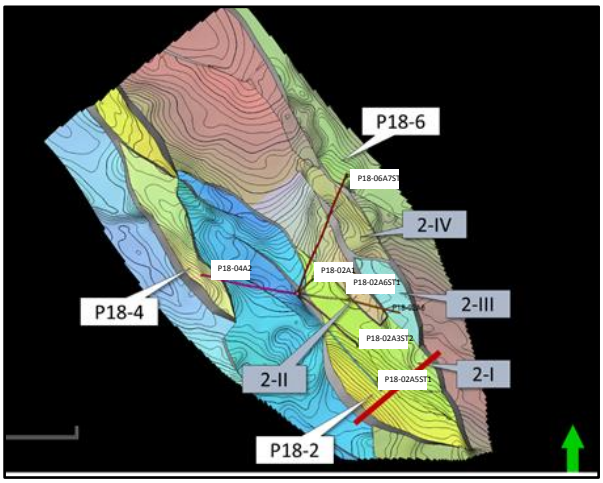

Figure 2: Overview of the three P18 fields (P18-2, P18-4, and P18-6), and the blocks of the P18-2 Field (2-I, 2-II, 2-III, and 2-IV). Red line indicates the position of the cross section shown in Figure 4 (TNO, 2019).

The reservoirs belong to the Triassic Buntsandstein and consist of the Hardegsen, Upper and Lower Detfurth and Volpriehausen. The tight Volpriehausen member gives only a small contribution to the reservoir storage capacity. However, the full reservoir height of some 220m is included in the geomechanical analyses since these layers may all deplete or repressurize over time. This is a conservative assumption for the seismic hazard evaluation.
Figure 4 shows a typical cross-section through the P18-2 field with the bounding faults on which significant stress concentrations can be expected during depletion of the field.

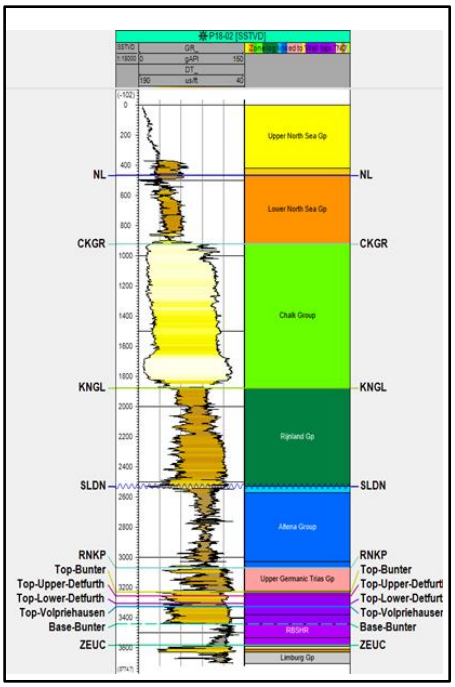

Figure 3: Lithology of the Triassic P18-2 field and overburden. The Hardegsen (Top Bunter) and Detfurth layers comprise the reservoir with a small contribution from the tight Volpriehausen layer (TNO, 2019).

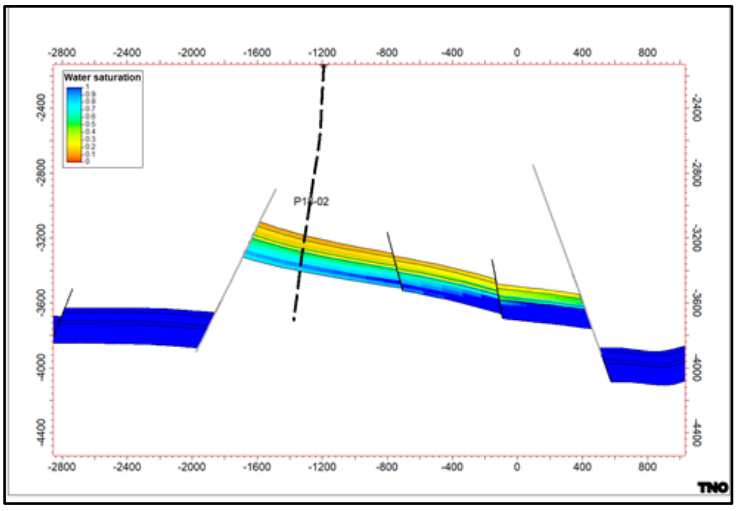

Figure 4: Cross section through the P18-2 field, showing block 2-I with initial water saturation. The location of the cross section is shown in Figure 2 (TNO, 2019).

The main concern with seismicity is not so much the potential damage to surface structures, which is in this case only a few nearby wellhead platforms that should be earthquake resistant. Slippage on faults might also enhance conductivity on faults which could lead to upward migration of CO2. Fortunately, the seal overlying the reservoir is 700m thick, so that the probability of any leakage through faults is negligible.
No seismicity has been observed during depletion of the field, which already reached a low pressure, so that seismicity could be expected. However, in the future the stress at the faults will differ from the historical stress, so that in principle an earthquake cannot be excluded.
Several methods will be used to estimate a maximum possible magnitude and the likelihood of such an event. Deterministic risk analysis will be applied to obtain the classification of P18 with respect to perceived risk in Dutch gas fields. Maximum depletion will indicate high risk; in addition, the modulus contrast between reservoir and overburden and the potentially slipping fault surface area will also be determined.
Upon CO2 injection, with increasing reservoir pressure the seismic risk is expected to decrease with elastic reservoir behavior, as the stress on the faults will decrease. One uncertainty is the stress recovery which might not be elastic. Another new factor is cooling by injection, since adiabatic expansion of the CO2 will cool the reservoir significantly. This is a recognized risk of injection projects and will be treated separately as one of the injection risk factors.
First, the risk matrix for surface and subsurface risk will be evaluated for differential compaction. Since the standard subsurface risk matrix does not cover injection projects, a separate risk matrix will be used for the perceived risks during injection. For instance, fracturing and thermal stress will also be discussed.
The risk analysis will be based on the design study by TNO and the geomechanical analysis in this report.

2 Mechanisms of seismicity

Fault Stability Criterion: Predicting Seismicity

In the Northern part of the Netherlands (i.e. excluding Brabant and Limburg), there is no record of natural earthquakes indicating that the region is tectonically relaxed, i.e. any strain rate must be very low and fault stress is far from critical. Induced earthquakes are regularly caused by reservoir depletion and compaction and a few earthquakes may have been caused by injection during waterflooding or by drilling losses. Compaction seismicity only occurs after significant pressure depletion of about 30% of virgin pressure (Roest *et al*, 1993; Bourne *et al.*, 2014). This confirms that Dutch gas fields have no critically stressed faults either at reservoir level or in the deep subsurface. Depletion of the P18 reservoirs will cause some faults to become critical, due to differential compaction. However, injection seismicity depends on critically stressed faults, so that faults with little throw will pose no risk for injection seismicity since they are far from critical.
The criterion for fault slip is simplified to the Mohr-Coulomb criterion, which predicts slippage when the ratio of shear stress to effective normal stress exceeds the friction coefficient:

$$R_{crit} = \frac{\tau}{\sigma_n - p} > \mu \qquad (1)$$

Where τ is the shear stress on the fault plane, σ_n is the normal stress and p is the local pore pressure. This shows that three factors could cause slippage: increase of shear stress, decrease of normal stress or increase of local pore pressure in the fault. For instance, depletion will increase the effective normal stress but the increase in shear stress caused by differential compaction can drive the fault into criticality.

Injection induced seismicity is most often caused by increasing pore pressure. This effect has been extensively observed in geothermal and waste water injection. In CO2 injection, cooling of the reservoir might play a significant role. Furthermore, it is also possible that stress due to opening an injection fracture causes fault instability.

In order to assess the maximum earthquake magnitude, it is necessary to consider the size of the slippage area on a fault since that determines the magnitude, as illustrated in Figure 5.

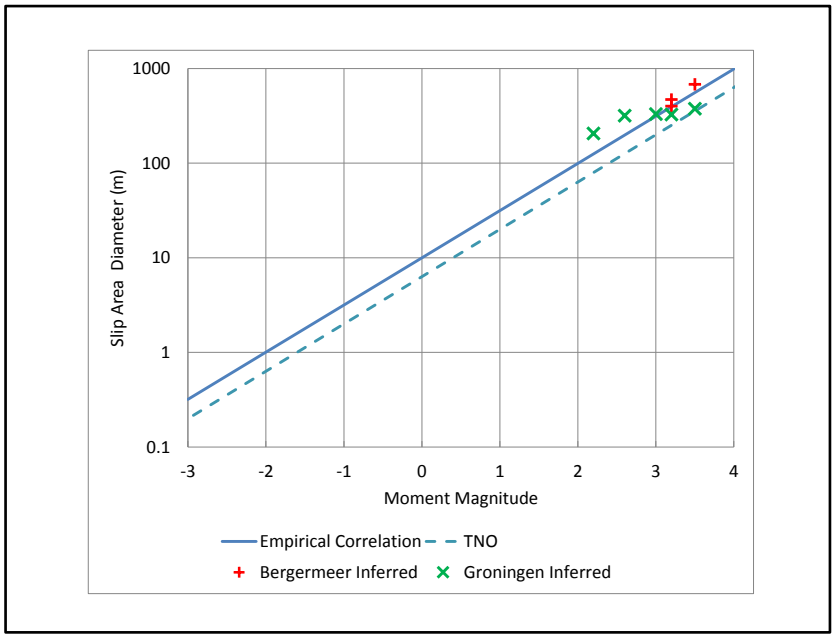

Figure 5: Correlation between size of rupture area (for a square area) and earthquake magnitude. Using seismic traces the size of the slip area and the stress drop can be inferred. These slip area dimensions are plotted for depletion earthquakes in Bergermeer and Groningen. For a computed maximum slip area, the empirical relation gives a conservative estimate of magnitude. The TNO correlation is based on a theoretical relation and is more conservative.

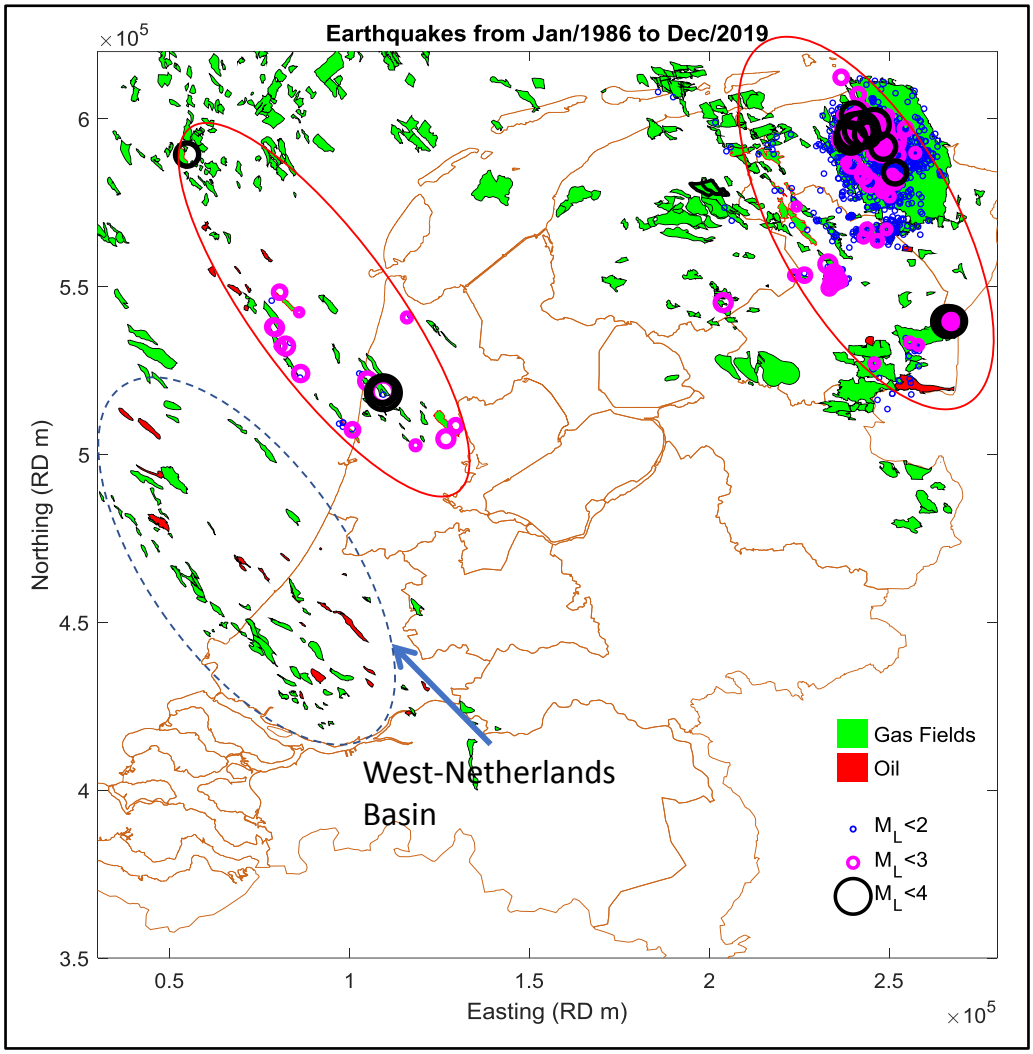

Figure 6: Map of gas fields in the Netherlands. Induced earthquakes in the Netherlands are concentrated in two areas: one near the Groningen gas field and another near the Bergermeer field and neighbouring fields that lie on the same trend. The P18 fields belong to a trend of gas fields, extending from Zuid-Holland to offshore P18 and P15 blocks (West-Netherlands Basin) that are seismically quiet.

Figure 6 shows induced seismicity in the Netherlands, which apparently occurs in two clusters of fields. It might be concluded that the gas fields in non-seismic areas just have no faults or faults that never become critically stressed, but that is not the case. The main causes of seismicity are the presence of faults in the reservoirs and significant compaction. A number of fields have such faults and significant depletion so that the faults become critically stressed, so that the absence of seismicity cannot be explained from reservoir properties (Vörös *et al.*, 2019). For instance, the Monster field is fully depleted, but induced no seismicity, while the seismic risk analysis could not exclude seismic risk; see NAM (2013), which assigns a probability of up to 42% for induced seismicity.

As yet, it is unclear what causes the regional variation of seismicity in Dutch gas fields and the non-seismic character of P18, but it can be concluded that even when the faults become critically stressed, the probability of seismicity is very low, since none of the fields in the West-Netherlands Basin have induced any seismicity.

3 Reservoir properties, pressure and fault system

The Buntsandstein reservoirs are conventional gas reservoirs with fairly good porosity and permeability, see Table 2. The modulus was determined from a Dipole Shear Sonic log, shown in Figure 7. The average value of the modulus over the reservoir is 37GPa, assuming a ratio of static to dynamic modulus of 75%. For seismic hazard, the ratio of overburden to reservoir modulus is important, so it does not matter how the dynamic modulus from sonic logs is converted to static modulus. However, compaction is proportional to the absolute value. We obtain a higher value of the modulus than used in the TNO study, but the lower estimate of 18 GPa will be used, which is equivalent to a conservative estimate of compaction.
From the density logs, LOT data and past fracture treatments in nearby fields, there is fair control of the vertical and minimum horizontal stress. The maximum horizontal stress is estimated from regional experience based on drilling data as fairly high but still lower than the vertical stress. The stress orientation was assumed to coincide with regional stress: maximum stress at 40degNW from data in the World Stress Map, see Figure 9.

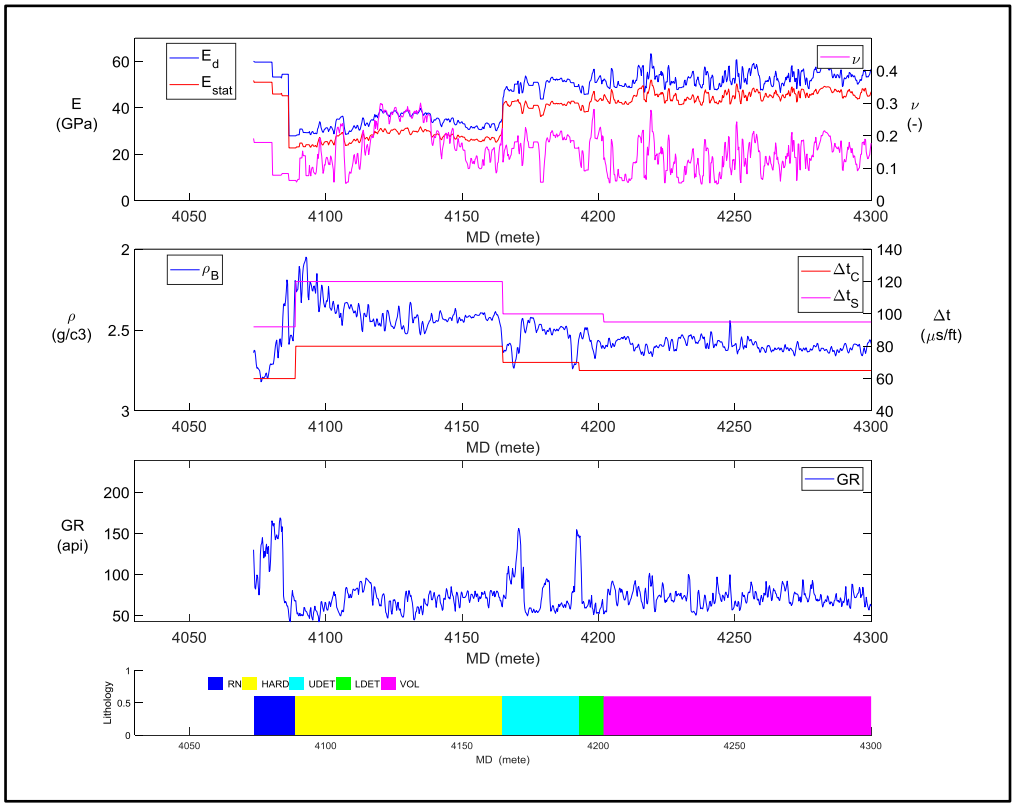

Figure 7: Logs and lithology in well P18-04A2. DSI readings from log displays were used to compute the modulus in overburden and reservoir. The Hardegsen reservoir has lower modulus than the overburden.

Table 1: Average reservoir properties. Most properties apply to all three fields, but the pressure and stress changes apply to P18-2. The pressure for the other fields is listed in Table 3.

Modulus			18	GPa	Virgin pressure	375	bar
Poisson ratio			0.25		Depleted pressure	20	bar
Biot Coefficient			1		Pressure drop	-355	bar
Compaction coefficient			0.046	1/GPa	Thermal expansion coefficient	1.00E-05	1/C
Depth			3500	m	Temperature drop	-90	C
Horizontal stress ratio			0.43		Thermal stress coefficient	2.4	bar/C
Stress path coefficient			0.60		Thermal stress drop	-216	bar
Vertical stress gradient			20.30	kPa/m	Poroelastic coefficient	0.67	
Minimum horizontal stress gradient			14.84	kPa/m	Poroelastic stress drop	-237	bar
Reservoir pressure gradient			10.71	kPa/m	Stress gradient drop	-6.8	kPa/m

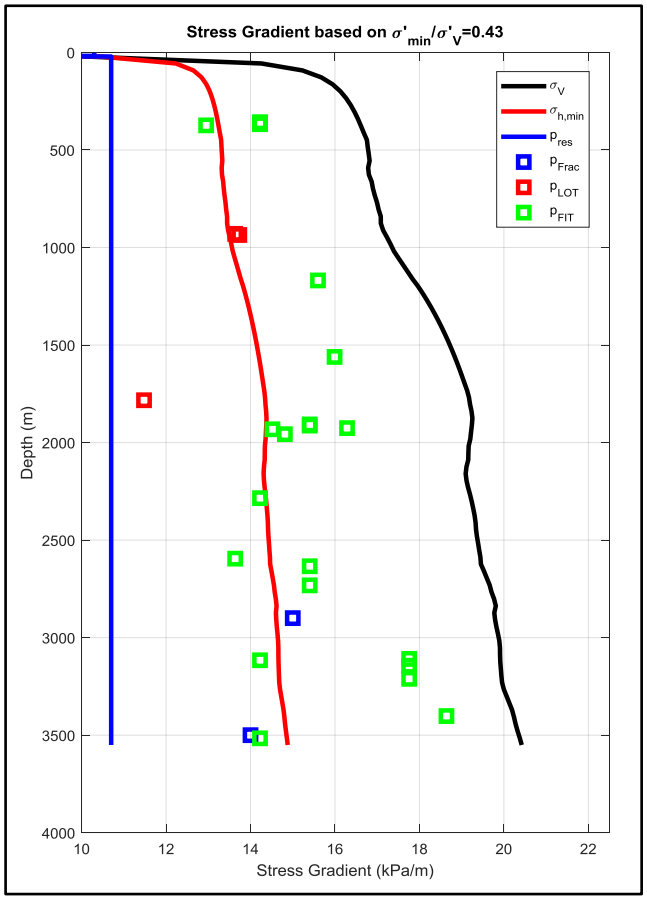

Figure 8: Stress gradients derived from P18-1 logs and LOT pressures as well as fracture gradients determined in nearby P15 and P12 fracture injection PFO's. The logs in the P18-2 well yielded the same result for the reservoir stress.

Table 2: Average properties of the reservoir layers.

	Thickness (m)	Porosity (BV)	Permeability (mD)
Hardegsen	20	0.11	154
Upper Detfurth	50	0.09	38
Lower Detfurth	30	0.07	31
Volpriehausen	85	0.03	0.02

Table 3: Reservoir pressures per field.

	P18-2 (bar)	P18-4 (bar)	P18-6 (bar)
Initial pressure	375	340	377
End production / start injection pressure	20	20	45
90 hydrostatic pressure	316	290	321
100 hydrostatic pressure	351	322	357
Initial pressure	375	340	377

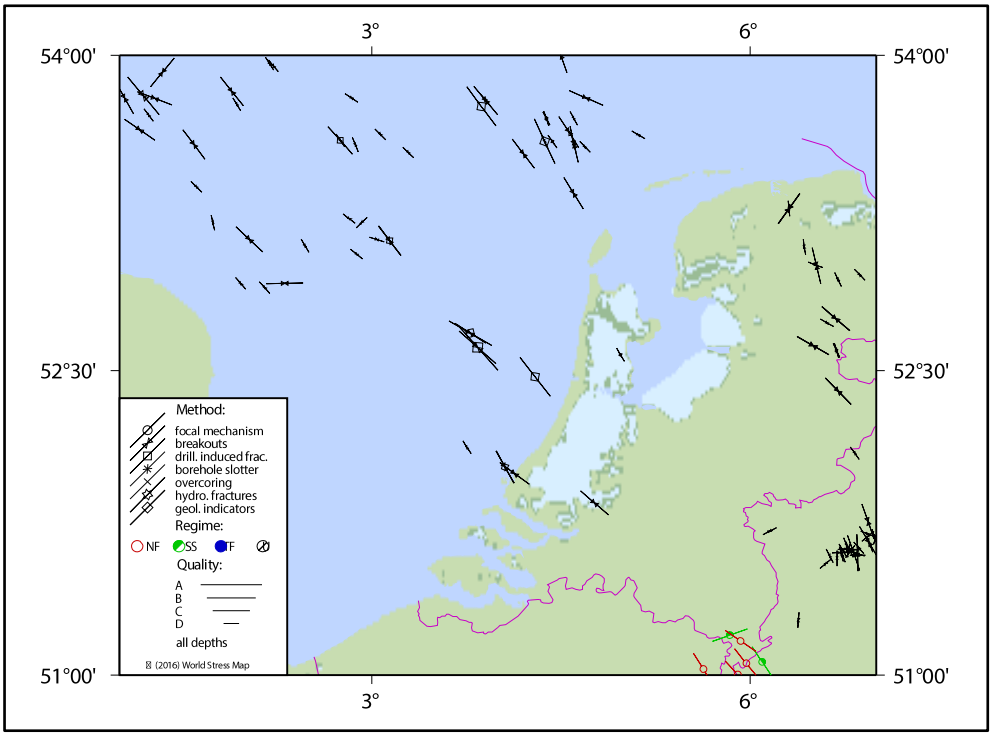

Figure 9: Stress orientation in the North Sea area near P18 (World Stress Map, 2016).

Fault System

Experience shows that stronger induced earthquakes occur on existing large faults that are activated by compaction or injection. So, it is important to determine the fault size and the distance of the wells from the main faults. This will be restricted to the faults mapped in the seismic interpretation, which only maps the larger faults.

The faults in the P18-2 field are shown in Figure 10. The cross-section through the main injector is shown in Figure 11. The boundary fault 10 is more than 600m from the well, but the intra-block fault 35 is 264m from the well. In the other fields the faults are also steeply dipping, striking close to the maximum stress orientation and some faults are within a few hundred meters from the injector, see Table 4. Fault 35 was not considered in the stress analysis of TNO (2019), since it has little offset, so that differential compaction is small. However, even a fault with little offset can be activated by injection pressure. It is therefore necessary to consider also the intra-reservoir faults for injection seismicity.

Most faults are striking along the maximum horizontal stress, which means that they are favourably oriented for slip. However, any hydrofracs will propagate along maximum stress along the faults, so the fractures would not propagate towards a fault.

In Table 4 the boundary faults that are close to injectors are indicated in yellow. These faults are of interest since depletion will induce high shear stress on these faults by differential compaction.

Table 4: Distance of injectors to nearby faults, within 1km distance. Distances were calculated from the centre of the Hardegsen interval. Yellow colour indicates boundary faults that have become stressed by differential compaction during depletion.

P18-02A5		P18-02A1		P18-02A3ST2		P18-04A2		P18-06A7ST1	
FN	Distance	FN	Distance	FN	Distance	FN	Distance	FN	Distance
P18-04-F35	264	P18-04-F14	234	P18-04-F35	271	P18-04-F01	226	Fault400	235
P18-04-F10	614	P18-04-F17	325	P18-04-F10	711	P18-04-F09	309	Fault600	413
P18-04-F24	687	P18-04-F10	341	P18-04-F17	722	P18-04-F13	490	Fault430	666
P18-04-F34	721	P18-04-F11	399						
P18-04-F32	829	P18-04-F13	893						
		P18-04-F19	932						
		Fault3	997						

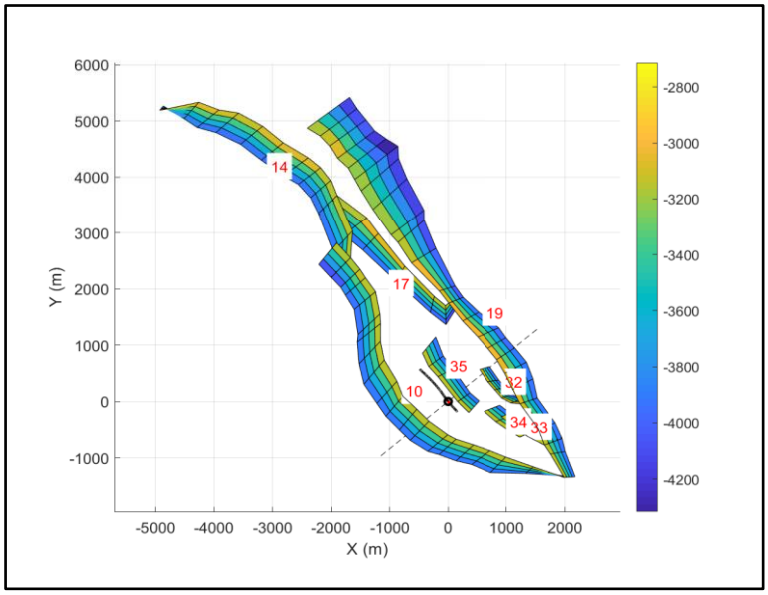

Figure 10: Faults in the P18-2 field, with well P18-2-A5. The dashed line indicates the cross-section along the minimum stress direction.

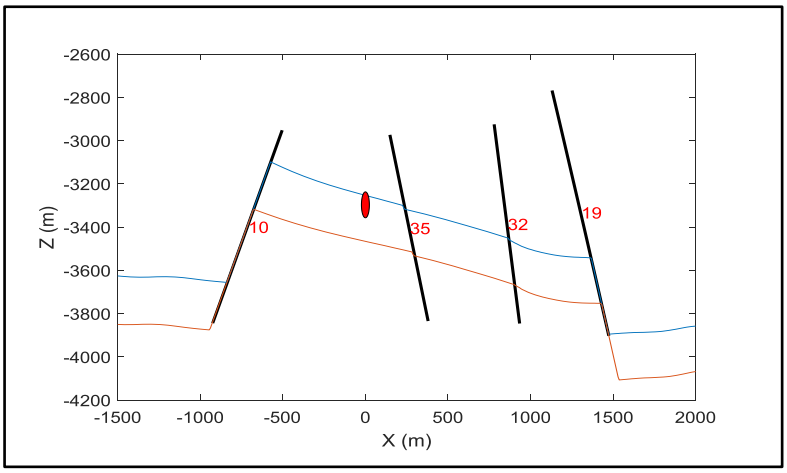

Figure 11: Faults in a cross-section through well P18-2-A5 along the minimum stress direction. The red ellipse indicates the injection interval.

Figure 12 shows the faults near well P18-02A1 and Figure 13 and Figure 14 shows the cross-section along minimum and maximum stress, respectively. This well is quite close to faults 14 and 10 that are boundary faults. These faults obtain high shear stress during depletion of the reservoir (TNO, 2019; Fig 7-2).

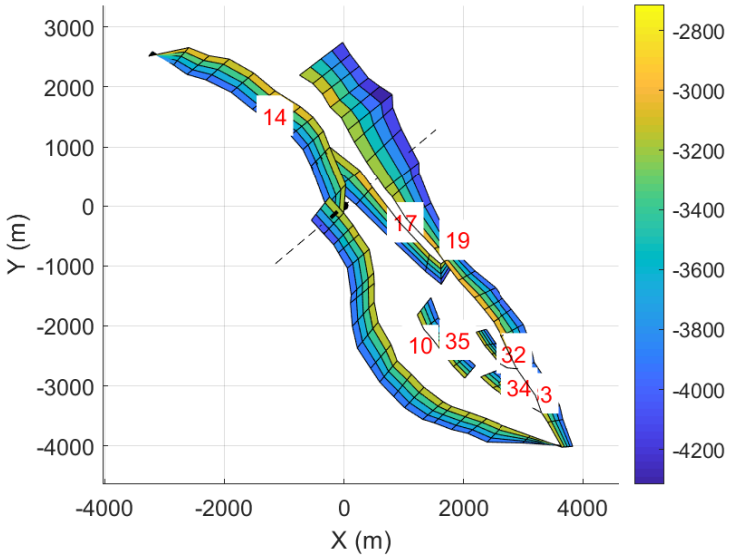

Figure 12: Faults in the P18-2 field, with well P18-2-A1. The dashed line indicates the cross-section along the maximum stress direction.

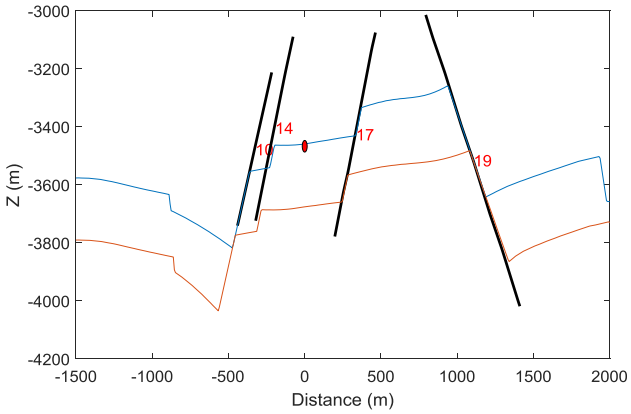

Figure 13: Faults in a cross-section through well P18-2A1 along the minimum stress direction. The red ellipse indicates the injector.

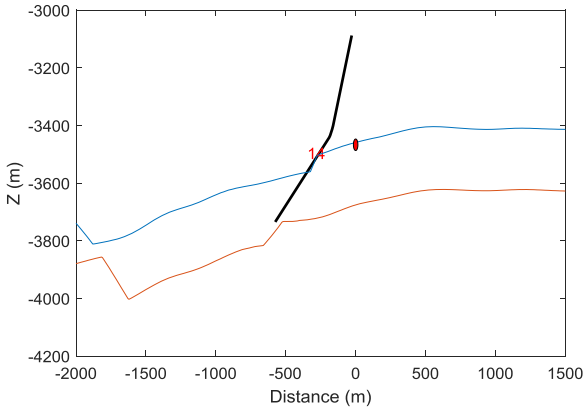

Figure 14: Faults in a cross-section through well P18-2A1 along the maximum stress direction. The red ellipse indicates the injector.

Figure 15 shows the faults near well P18-02A3. This well is far from boundary faults, as shown in Figure 16 and Figure 17. The tip of Fault35 is fairly close, but this is an intra-reservoir faults with small throw.

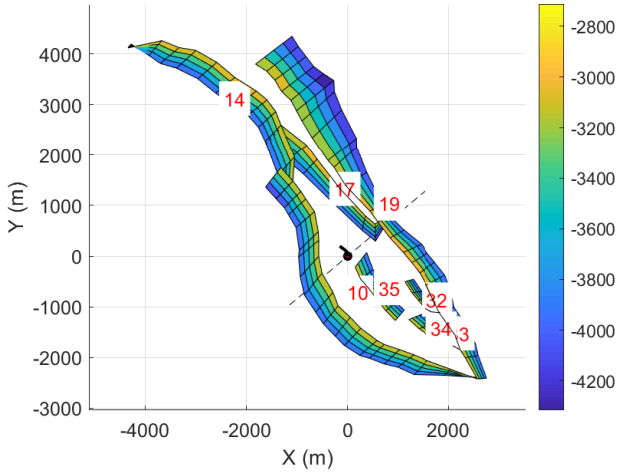

Figure 15: Faults in the P18-2 field, with well P18-2A3. The dashed line indicates the cross-section along the minimum stress direction.

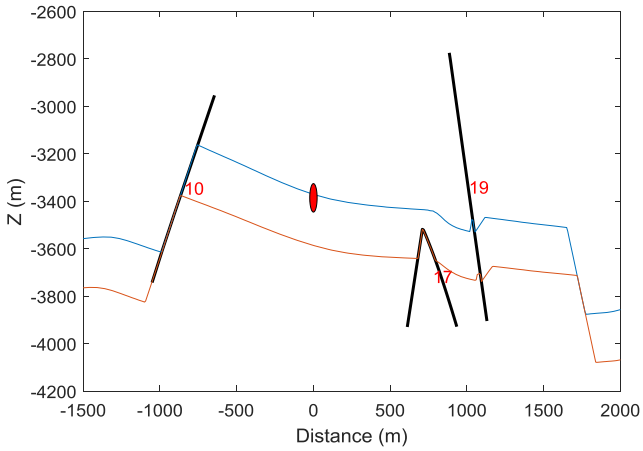

Figure 16: Faults in a cross-section through well P18-2A3 along the minimum stress direction. The red ellipse indicates the injector.

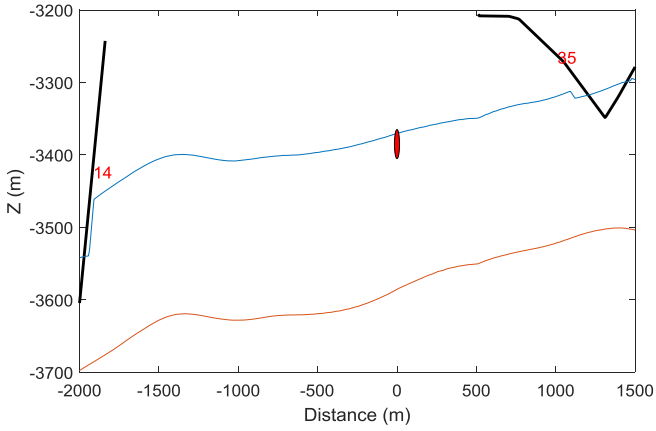

Figure 17: Faults in a cross-section through well P18-2A3 along the maximum stress direction. The red ellipse indicates the injector.

Figure 18 shows the faults that bound the P18-4 field. The cross section is shown in Figure 19.

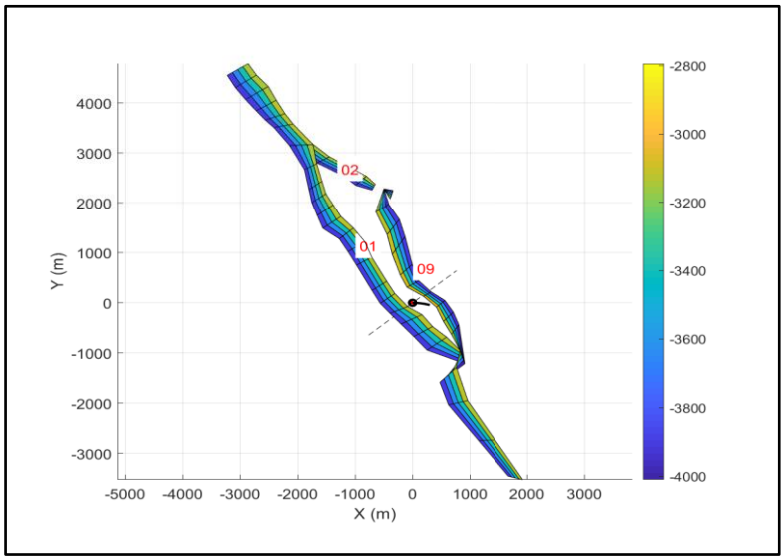

Figure 18: Faults in the P18-4 field, with well P18-4A2. The dashed line indicates the cross-section along the minimum stress direction.

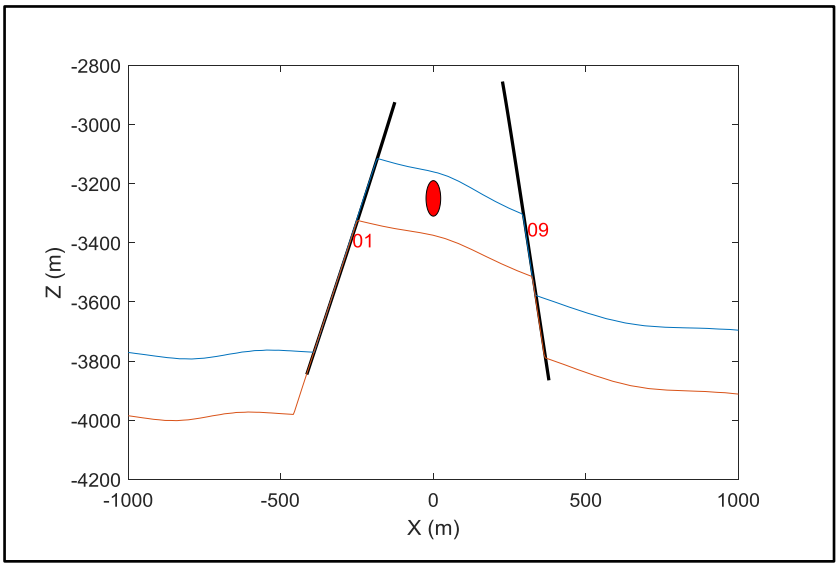

Figure 19: Faults in the P18-4 field, in a cross-section through well P18-4A2 along the minimum stress direction. The red ellipse indicates the Injection interval in well.

Figure 20 shows the P18-6 field faults with cross-section along minimum stress shown in Figure 21. The well is close to the bounding fault 400. Since this is a small field with limited gas zone, the compaction will be small, so that differential compaction will be limited.

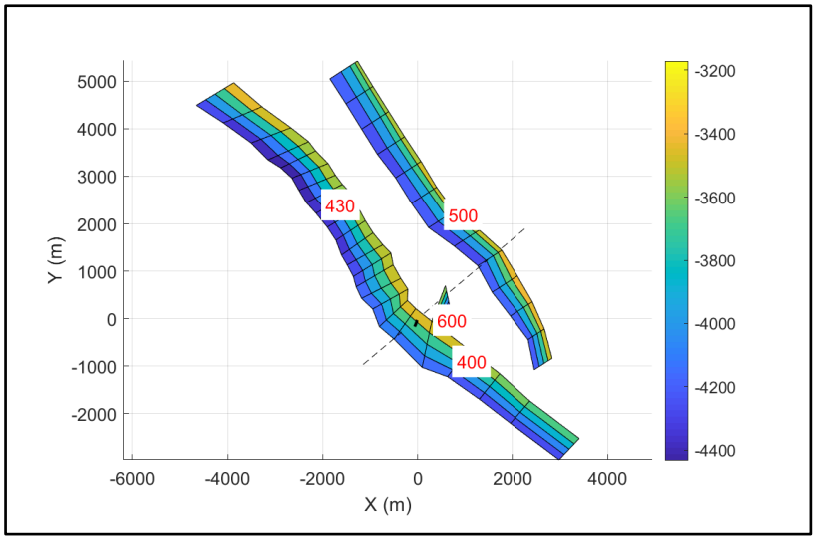

Figure 20: Faults in the P18-6 field, with well P18-6A7ST1. The dashed line indicates the cross-section along the minimum stress direction.

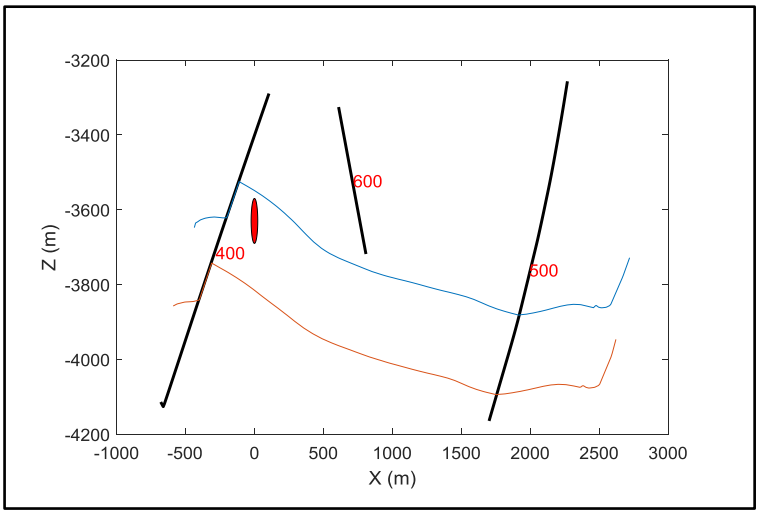

Figure 21: Faults in a cross-section through well P18-6A7ST1 along the minimum stress direction. The red ellipse indicates the injector.

4 Stress Analysis

Virgin Stress and Pore Pressure Effect

Stability of the faults near the well may be influenced by the injection pressure and cooling. First, the stress on the faults in the virgin condition will be analysed. Stability depends on the normal and shear stress on the fault planes. Most faults have a favourable orientation in the stress field, so that the vertical and minimum stress give a large shear stress on the fault. From the fault stability condition, Eqn 1, the excess pressure above reservoir pressure can be computed that would destabilize the fault. This is shown in Figure 22 for virgin stress. In the depleted state the critical pressure is plotted in Figure 23. In these figures, each point in the polar diagram represents the normal to a fault plane. The origin of the plot is the horizontal plane, while the boundary represents vertical planes with different strike. The crosses represent the well axis and the circles correspond with faults in the vicinity of the main injector, P18-2A5, see cross-section Figure 11.

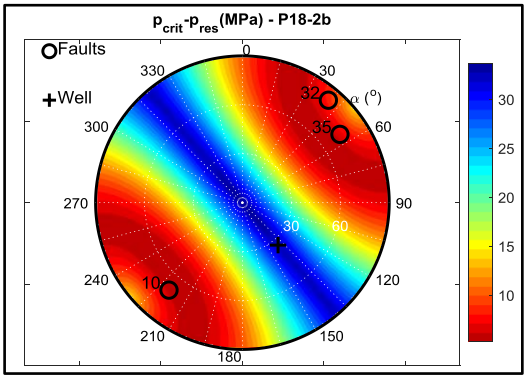

Figure 22: Critical excess pressure above reservoir pressure that is needed to destabilize a fault in the virgin state.

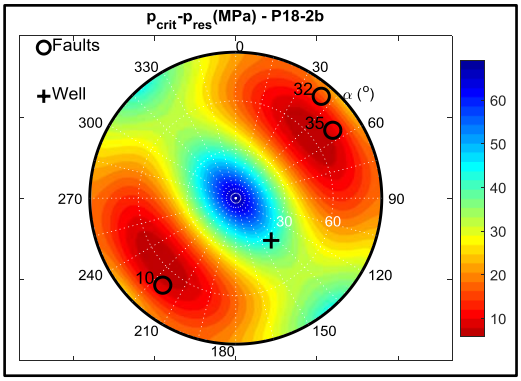

Figure 23: Critical excess pressure above reservoir pressure that is needed to destabilize a fault, after depletion.

Assuming a favourably oriented fault, the critical excess pressure would be 5.3MPa as shown in the Mohr circle diagram in Figure 24. The pressure at the fracture entrance is just 3-4 MPa above reservoir pressure (TNO, 2019, pp51-52), so the fracture pressure should be insufficient to destabilize a fault. Moreover, the injection pressure extends only over a small area, since the pressure falls off quickly away from the injector.
Figure 25 shows the effect of depletion and cooling. The Mohr diagram confirms that depletion does not have a big effect on stability of the reservoir faults. Of course, differential compaction at the boundaries of reservoir with non-reservoir rock is not captured by the stress changes shown in Figure 25, which only apply to intra-reservoir faults with little offset, such as Fault35. The TNO study indeed showed that some sections of the boundary faults become critically stressed due to reservoir compaction.
Cooling has a much stronger effect on reservoir faults, since the horizontal stress is expected to decrease strongly. The reservoir will not reach the thermal fracturing regime (with negative effective stress), but the confining stress will become very low so that slippage is possible, even for a modest level of the shear stress, shown in Figure 25. For a thermal expansion coefficient of 10^{-5} and 90°C cooling, the stress reduction is about 21MPa, which translates in a Mohr-Coulomb stress increase of about 10MPa. The critical stress would then

be just reached for a cooling of 20°C. Since the TNO study showed that the cooling front can extend several hundred meter form the well, it is likely that the cold zone can reach some faults. TNO (2019) computed the extent of the cold front for the main injector, which is far from the boundary faults. The other injectors are much closer to boundary faults, but these wells inject at a rate that is more than 8 times lower. That gives at least an 8 times slower cold front penetration, so the cold front will not reach the faults in the first years when injection pressure is highest. At the end of the injection project, the pressure is restored which stabilizes the boundary faults, the injection pressure is lower and the cooling effect will be reduced because adiabatic expansion is diminished by the higher background pressure.
The cooling presents a new risk since the reservoir has not been cooled in the past, but the critically stressed faults will not be cooled during the first years of the injection. Therefore, the risk of thermally induced seismicity is negligible.

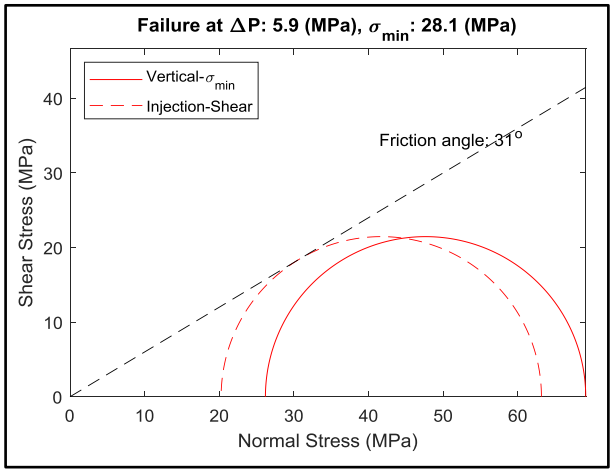

Figure 24: Mohr Coulomb plot for stresses after depletion in the P18-2 reservoir. For a critically oriented fault, instability could occur with an excess pressure of 5.3MPa in the fault

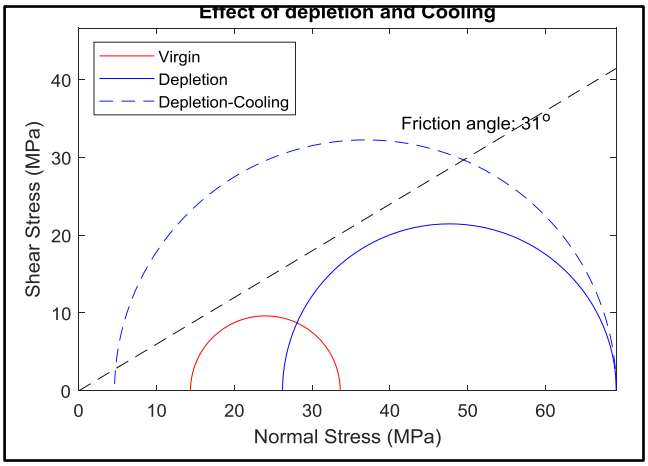

Figure 25: Mohr Coulomb plot for virgin stresses in the P18-2 reservoir. Also, the effect of depletion and cooling by CO2 injection is plotted.

5 Fracture Simulations

For seismic risk due to injection, an important issue is fracture propagation at the injectors, since a long fracture could not only cause increased pressure at a fault, but also modify the thermal front so that cooling occurs over longer distances. Although injection pressure is quite low, it is still of interest to consider fracture propagation by thermal stress reduction. Simple fracture simulations were performed in 2D using elliptical flow geometry (Hagoort, 1980; Koning, 1988). Only the first year is simulated, since it will be very uncertain to make a long-term forecast. It is assumed that the reservoir is cooled by 90ºC and the injection rate is used for the main injector, P18-2A5. The cooling by CO2 injection happens not only due to the heat capacity of the fluid, but mainly by Joule-Thompson expansion. This effect was added to the thermal model, which was developed for water injection. The simulations were benchmarked to the TOUGH2 simulations by TNO which model the entire thermodynamics of CO2 injection. The model considers only 100 m reservoir consisting of Hardegsen and Detfurth; the resulting pressure of 3.5 MPa above reservoir pressure matches the TNO results (TNO, 2019, pp52-52). The cooling simulation is shown in TNO (2019; pp 66, Fig 7-7). For the standard input parameters, no fracture is propagated, since the stress remains far above the injection pressure, see Figure 26.

However, the thermal stress depends on the coefficient of thermal expansion (taken as $10^{-5}C^{-1}$) and the modulus, which could be higher than the estimated value of 18 GPa. The modulus of sandstones with the porosity of the Hardegsen is commonly about 30GPa (English, 2019). For Buntsandstein sandstones Heap (2019) found an average modulus of 25GPa at a porosity of 11%, with a range of 5GPa.

For a higher value of the modulus of 30GPa, the thermal stress reduction is larger and a fracture can be propagated, see Figure 27, Figure 28 and Figure 29. The pressure distribution is hardly affected by the fracture, but the cooled region becomes somewhat elliptical. For these conditions the fracture size is moderate and the cold zone remains almost circular. Quite often, thermal fractures have only an impact on the injectivity and not on the shape of the flood front because both horizontal stresses become very low, so that a fracture network is formed that keeps the flood front circular. However, when the maximum horizontal stress is much larger than the minimum stress, the cold front becomes elliptical with a length that is much larger than the width. No evidence exists for a large horizontal stress difference so that a single fracture

Since the fracture propagates due to cooling it will also be strongly contained in the layers that accept the injected CO2. Therefore, there is no risk of upward or downward fracture growth.

Fortunately, the maximum stress orientation is along the major faults, so any fracture would propagate along the faults. Therefore, it is unlikely that a fracture would ever hit a fault. Well P18-2A1 is close to a fault as listed in Table 4, but that well has a much lower injection rate, so that less cooling and even lower injection pressure is expected so that no fracture propagation is possible.

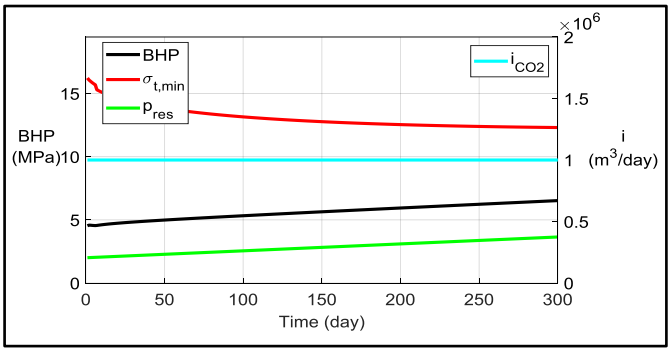

Figure 26: Pressure in base case fracture simulation for CO2 injection into P18-2 field. Since the pressure is much lower than the stress, no fracture propagation is possible. Only if the thermal stress would fall below the BHP a fracture could propagate.

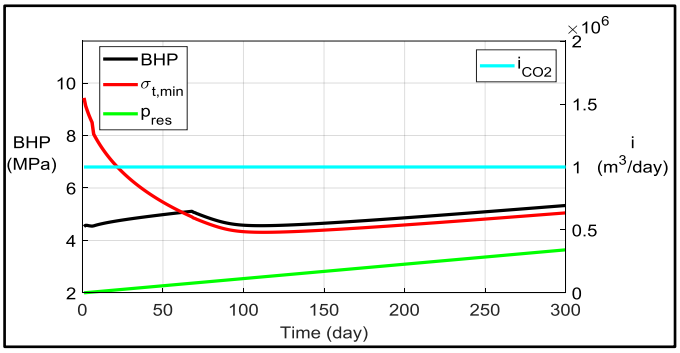

Figure 27: Pressure in fracture simulation for CO2 injection into P18-2 field for higher modulus of 30GPa. Since thermal stress is proportional to the modulus, the lower stress facilitates fracturing after a few months injection.

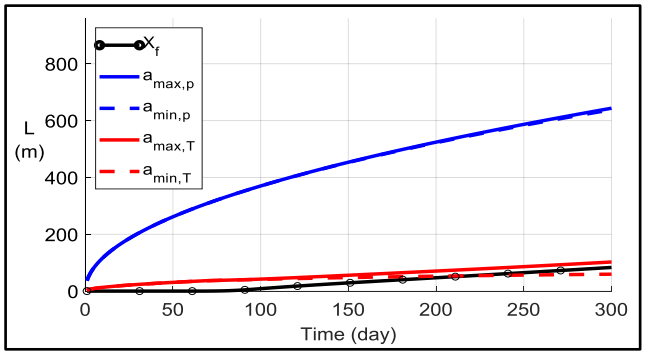

Figure 28: pressure and temperature fronts in the simulation with fracturing. In agreement with detailed CO2 simulations, the cold front extends over several hundred meters after 5 years and after 1 year the extent is some 50 m which facilitates an 80 m fracture length.

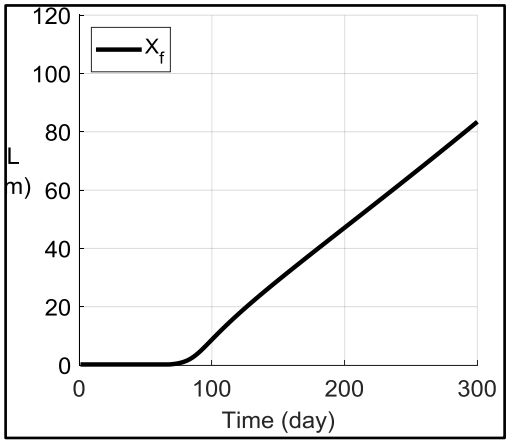

Figure 29: Fracture size vs. time, for simulation with high modulus of 30GPa.

For the P18-2 injector, fracturing can be monitored by observing the excess injection pressure (over reservoir pressure), which should rise with time. If injectivity improves, it is an indication of fracturing, so that fracture size should be monitored. It may be feasible to infer fracture size from the injectivity, but the pressure behavior is likely insensitive to fracture size and the usual method of inferring fracture size from Pressure fall-offs is complicated by the phase behavior of the CO2. The most important effect may be a larger extent of the cold front compared with matrix injection. This could cause earlier cooling at nearby faults and some pressure increase at a fault. However, since injection pressure is low compared with reservoir stress, the effect of fracture pressure on the faults will be negligible.

6 Risk Analysis

Deterministic Seismic Hazard Analysis

For compaction induced seismicity, the SoDM guideline suggests risk factors for subsurface processes based on a deterministic analysis and a few other factors. Most important is the pressure depletion, for which a threshold of 30% depletion has been determined before the onset of seismicity. P18 fields have been almost completely depleted so this factor is satisfied. The contrast between reservoir stiffness and non-reservoir stiffness is another factor, since differential compaction depends on this ratio. Table 5 lists the modulus of reservoir and overburden: the modulus ratio is 1.3, which exceeds the threshold for seismicity of 1. The E-ratio is just below the upper threshold of 1.34, but it is so close that the highest risk is assigned, which is a conservative approach. Since faults are essential for seismicity, the degree of faulting is another factor. Table 6 lists the ratio of fault area to reservoir volume which results in B-factors for the fields that exceed the threshold for seismicity of 0.86. This would put the P18 reservoirs in the highest seismicity risk class of 42%. The B-factor is computed from fault length, L, reservoir volume, V and reservoir height, H with:

$$B = \frac{H_{res} \sum_{faults} L_{fault,i}}{V_{res}^{2/3}} \tag{2}$$

These factors indicate higher risk of relatively strong seismicity. The combined Risk Index is computed with the sum of all scores, s_i:

$$I_R = \frac{\sum_{All} s_i}{\sum_{All} \max(s_i)} \tag{3}$$

Table 9 lists the risk factors and scores for the P18 field. Table 10 gives the surface risk factors, which were developed for onshore fields. For offshore fields the vulnerability of surface structures concerns only the nearby wellhead platforms, which are of course earthquake resistant, since their foundations are built to withstand North Sea storms. Here, the guideline by SoDM is followed, which specifies an influence radius of 5km.

Both subsurface and surface risk indices can be combined to derive the risk class, as plotted in Figure 30. Clearly, the field falls in the negligible risk class.

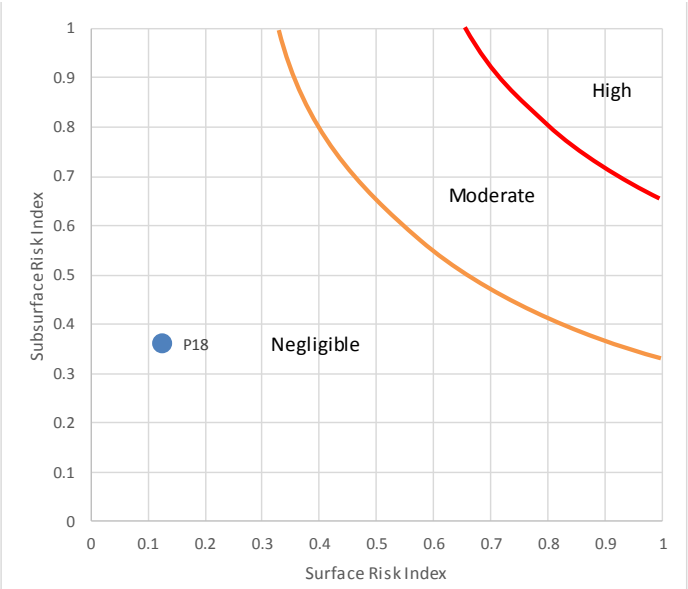

Figure 30: Risk map with surface risk index on the horizontal axis and subsurface risk index on the vertical axis.

Table 5: Modulus from DSI log in P18-4 well, with E-factor.

	Top (m)	ρ_B (g/c3)	Δt_C (ms/ft)	Δt_S (\mus/ft)	E_{dyn} (GPa)	E_{stat} (GPa)	ν (-)
RN	4076	2.67	60	92	56.5	48.3	0.13
HARD	4093	2.40	80	120	34.0	27.6	0.18
UDET	4166	2.52	70	100	50.0	41.0	0.17
LDET	4194	2.57	65	100	50.7	42.1	0.18
VOL	4209	2.59	65	95	52.8	45.3	0.13
					E-ratio	1.31	

Table 6: Total fault length and block volume for P18-2, P18-4 and P18-6 fields with the corresponding B-factor. The B-factor was also computed including only the boundary faults, which are most significant, but that yielded also a high value.

Block	L (m)	L-Boundary (m)	Hres (m)	Vres (m^3)	B (-)	B-boundary (-)
P18-2	2.01E+04	1.61E+04	210	2.71E+09	3.2	2.3
P18-4	1.07E+04	1.07E+04	229	6.23E+08	6.2	6.2
P18-6	1.95E+04	1.95E+04	228	5.07E+09	1.9	1.9

Table 7: Fault length and maximum magnitude of earthquakes that could be sustained by each fault.

	# 0	Length (m)	M0 (Nm)	M (-)
P18-2	10	6378.6	1.50E+15	4.1
	14	1180.9	2.78E+14	3.6
	17	3144.1	7.41E+14	3.8
	19	5363.8	1.26E+15	4.0
	32	1022.7	2.41E+14	3.5
	33	890.5	2.10E+14	3.5
	34	765.2	1.80E+14	3.4
	35	1350.0	3.18E+14	3.6
P18-4	1	5235.8	1.23E+15	4.0
	2	1519.0	3.58E+14	3.6
	9	3941.7	9.29E+14	3.9
P18-6	129	7588.2	1.79E+15	4.1
	130	5784.5	1.36E+15	4.0
	131	4997.0	1.18E+15	4.0
	134	1106.3	2.61E+14	3.5
	130-131	10781.4	2.54E+15	4.2

Table 8: Reservoir bulk volumes and maximum magnitude that could be induced based on the compaction energy release. For P18-2 and P18-4 the volume change was computed assuming uniform pressure at full depletion. For P18-6 the volume change was computed with the simulated pressure at full depletion. Since most of the bulk volume of P18-6 experiences no pressure decrease, the volume change is relatively small.

	FIPNUM	Volume	Area	Height	δVolume	M_0	M
	(-)	(m3)	(m2)	(m)	(m3)	(Nm)	(-)
P18-2	4	1.57E+09	7.11E+06	220	2.58E+06	2.47E+14	
P18-2	11	7.68E+08	3.05E+06	252	1.26E+06	1.21E+14	
P18-2	6	3.05E+08	1.43E+06	214	5.01E+05	4.81E+13	
P18-2	10	2.85E+08	1.33E+06	214	4.69E+05	4.50E+13	3.7
P18-4	2	6.23E+08	2.72E+06	229	1.02E+06	9.83E+13	3.3
P18-6		5.07E+09	2.22E+07	228	5.22E+05	5.01E+13	3.1

Table 9: Subsurface risk factors for seismicity

	DHAIS	M	Ligging voorkomen	Opslingering	Score
5		Alle methodes >4,5			
4	Bevend veld > 5 bevingen per jaar van M≥ 1,5	1 methode > 4,5 én/of Alle methodes 4,1 – 4,5			
3	Bevend veld < 5 bevingen per jaar van M≥ 1,5	1 methode 4,1 – 4,5 én/of Alle methodes 3,6 – 4,0		>60% slappe grond (Vs,30 =< 200m/s) en/of >30% grondsoort die extra gevoelig zijn voor amplificatie, zoals veenlagen dikker dan 3m en slappe veenlagen met een dikte van 1m-3m gelegen op een stijve ondergrond.	
2	P=42% Of Bevend veld M < 1,5	1 methode 3,6 – 4,0 én/of Alle methodes 3,1 – 3,5	Boven de lijn Amsterdam-Arnhem	30-60% slappe grond (Vs,30 =< 200m/s) en/of 15-30% grondsoort die extra gevoelig zijn voor amplificatie, zoals veenlagen dikker dan 3m en slappe veenlagen met een dikte van 1m-3m gelegen op een stijve ondergrond.	
1	P=19%	1 methode 3,1 – 3,5 én/of Alle methodes 2,6 – 3,0		10-30% slappe grond (Vs,30 =< 200m/s) en/of 5-15% grondsoort die extra gevoelig zijn voor amplificatie, zoals veenlagen dikker dan 3m en slappe veenlagen met een dikte van 1m-3m gelegen op een stijve ondergrond.	
0		1 methode 2,6 – 3,0 én/of Alle methodes ≤ 2,5	Onder de lijn Amsterdam-Arnhem	<10 % slappe grond (Vs,30 =< 200m/s) en/of < 5% grondsoort die extra gevoelig zijn voor amplificatie, zoals veenlagen dikker dan 3m en slappe veenlagen met een dikte van 1m-3m gelegen op een stijve ondergrond.	
	4	5	2	3	14
P18	2	3	0	0	0.36

Table 10: Surface risk factors. The factor for industrial installations was assigned 2, to allow for more platforms or other structures although at the moment no other platforms exist within 5km of the P18 field.

	Bevolkingsdichtheid (aantal inwoners per km2)	Industriële inrichtingen	Speciale gebouwen En vitale infrastructuur	Dijken	Sum/ Score
4	> 2500	Meerdere direct boven het veld	Meerder ziekenhuizen en/of energievoorzieningen direct boven het veld	Primaire dijken boven het veld	
3	1000-2500 en/of 500-1000 met wijken bestaande uit flats/ appartementen-complexen binnen 5 km rond het veld	1 boven het veld en/of meerdere binnen 5 km rond het veld.	1 ziekenhuis en/of energievoorziening direct boven het veld of meerdere binnen 5 km rond het veld. Meerdere scholen, tehuizen en/of publieksgebouwen direct boven het veld	Primaire dijken binnen 5 km rond het veld en/of secundaire dijken boven het veld	
2	500-1000 en/of 250-500 met wijken bestaande uit flats/ appartementen-complexen binnen 5 km rond het veld	1 binnen 5 km rond het veld.	1 school, tehuis en/of publieksgebouw boven het veld of meerdere binnen 5 km rond het veld.	Secundaire dijken binnen 5 km rond het veld	
1	250-500 en/of <250 met wijken bestaande uit flats/appartementen-complexen binnen 5 km rond het veld	-	1 school, tehuis en/of publieksgebouw binnen 5 km rond het veld.	-	
0	< 250	Geen binnen 5 km rond het veld	Geen boven en/of binnen 5 km rond het veld	Geen dijken binnen 5 km rond het veld	
Max	4	4	4	4	16
Weight	1	1	1	1	
P18	0	3	0	0	0.2
In Salah	1	2	1	0	0.25
Sleipner	0	2	0	0	0.125
Weyburn	1	2	1	0	0.25

Injection Seismicity Risk Analysis

The potential mechanisms of earthquakes generation by fluid injection have been reviewed by TNO (2014). These are:

- Poro-elastic stress effects as a result of the injection
- Pore pressure increase in a near-critically stressed fault
- Chemical reactions reducing the strength of a fault
- Thermal changes effecting stresses
- Mass changes
- Stress transfer from nearby earthquakes

For long-term injection chemical reactions and mass changes may be relevant but detailed lab studies have shown that chemical interaction of CO2 with sandstone is negligible (TNO, 2019) and the effect of mass changes can also be neglected since there are no deep fault systems that could be triggered by the additional mass of the CO2 compared with the virgin reservoir. Since the P18 field is in a seismically quiet area the stress transfer effect can be disregarded.

From water injection projects it is known that thermal stress change may become significant after some months. So, for the long-term injection of CO2 in a relatively stiff reservoir thermal stress reduction will play a role. Cooling occurs mainly because of Joule-Thomson effect during expansion of the injected CO2 into the low-pressure reservoir. Simulations by TNO (2019) have shown that the cold front can extend to faults near the injectors. The stress analysis of Figure 25 indicates that slippage may occur because of the reduction in confining stress on the faults.
In some German geothermal projects, seismicity started after injecting for years, which can be explained by cooling of the rock. The well-known Geysers geothermal project shows seismicity that is also presumed to be induced by thermal stress reduction.

For Geothermal injection the following risk factors were identified (Baisch *et al.*, 2014):

- basement connected
- inter-well pressure communication
- re-injection pressure [MPa]
- circulation rate [m^3/h]
- epicentral distance to natural earth-quakes [km]
- epicentral distance to induced seismicity [km]
- distance to fault [km]
- orientation of fault in current stress field net injected volume [1000 m3]

This is aimed at geothermal doublets, although some factors are relevant to all injection projects such as natural seismic activity and proximity to faults.

Experience with injection seismicity, has shown that the factors that govern injection seismicity risk are:

- Natural Seismicity: in seismically quiet regions strong injection seismicity is unlikely, as observed for instance in the Northern Netherlands (Foulger *et al.*, 2019). TNO (2014) found no evidence for felt induced seismicity by Dutch fracture treatments.
- Fault Density/ Location: seismic faults are necessary for induced seismicity
- Stress Regime: Felt induced injection seismicity is almost always observed in strike-slip or reverse faulting stress regimes (Foulger *et al.*, 2019).
- Reservoir Transmissibility and Storage Capacity: Pressure changes are the principal driver of geomechanical changes in CO2 storage reservoirs, so if any pressure change is small the effects will be small. A CCS project like Sleipner with injection into a huge aquifer where the total injected CO2 occupies only a tiny fraction of a percent of total storage volume is possibly the best option (Verdon, 2013).

In the P18 reservoirs the faults are likely critically stressed over some sections by differential compaction (TNO, 2019), which might be a risk factor for injection seismicity. However, the absence of seismicity shows

that these faults do not slip in a seismic mode. Therefore, the stressed state of these faults should not be considered as higher risk for injection.

Other factors that enhance risk are:

- Injection Volume: it has been observed that in cases where seismicity is induced the earthquakes get stronger for larger injection volume (McGarr, 1976).
- Thermal Stress reduction

Proximity to basement is a risk factors for injection seismicity, but this is irrelevant for CO2 injection since no projects exist near basement. Injection volumes are necessarily huge, which presents a significant seismic hazard, but it applies to all CCS projects. The qualification is that the large volume should not be associated with large pressure changes that could cause large earthquakes. A project like Sleipner has very small pressure changes because it injects into a huge aquifer, while In Salah has higher risk because injection induces large pressure changes.

As shown in the section on stress analysis, the main injector is far from any critically stressed faults, so thermal stress will not be relevant. Some minor injectors are close to intra-reservoir faults, but these are not stressed by differential compaction because the throw is small. Therefore, thermal stress effects will be insignificant.

These factors indicate higher risk of relatively strong seismicity. Therefore, the Injection Risk Index is computed with:

$$I_R = \frac{\sum_{All} W_i s_i}{\sum_{All} W_i \max\left(s_i\right)}, \tag{4}$$

Where s_i: risk score, W_i: weight factor.

Table 11 lists the risk factors and scores for the P18 reservoir. Unfortunately, there is no experience in the Netherlands with CO2 storage, so it is impossible to compare P18 with nearby CCS projects in the same geological setting. So, for reference, a few well-documented CO2 injection projects are added in other areas; some of these have induced seismicity, such as In Salah and Weyburn, Canada, while the Sleipner project in the North Sea showed no seismicity. Reviews of the In Salah, Sleipner and the Weyburn CO2 injection projects are presented by Verdon (2013) and Foulger *et al*. (2018). Sleipner is offshore, while In Salah is in the Algerian desert and Weyburn is in a remote area of Saskatchewan, Canada. Therefore, all three projects present low surface risk, but the storage reservoirs are quite different. Sleipner injects into a large, high-permeability aquifer, so that pressure changes are negligible. Weyburn is a hydrocarbon reservoir with complex stress history where CO2 is not only stored but also injected for EOR. In Salah is a fairly low-permeability aquifer with limited storage capacity that showed significant pressure increase. Both Weyburn and In Salah have induced weak seismicity of magnitude -1.0 and 1.7, respectively.

Figure 31 shows the risk classes for P18 and the reference cases. Calibration of this classification was based on the documented cases. It can be concluded that the P18 injection project falls in the class with negligible risk, analogous to Sleipner. Both the subsurface conditions indicate very low risk of seismic fault slippage over a large area and the surface risk is also negligible since only a few wellhead platforms are in the range of potential earthquake vibrations.

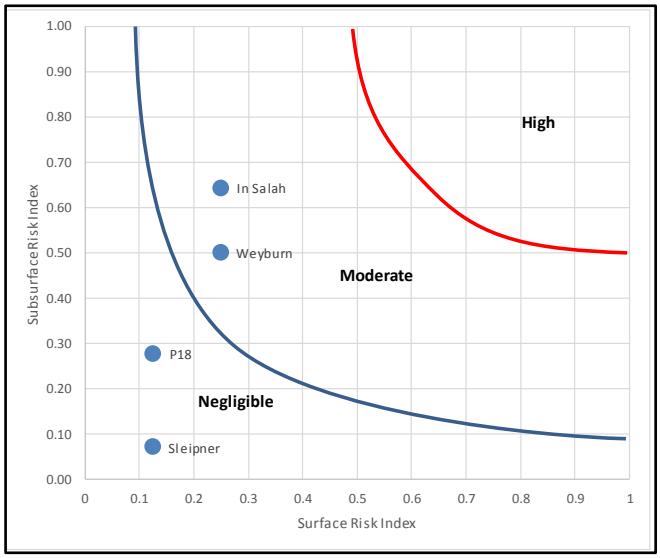

Figure 31: Risk map for injection seismicity with surface risk index on the horizontal axis and subsurface risk index on the vertical axis.

Table 11: Subsurface risk factors for injection seismicity. The weight factor recognizes the large significance of reservoir type for overall risk.

Code	Natural Seismicity	Fracture Density/ Location	Stress Regime	Reservoir Type	Thermal Stress	Score
3						
2	Active: M>6	Near active faults	Overthrust	Aquifer: Increased Pressure	Thermal Fracturing regime	-
1	Moderate: M=3	Many reservoir faults; No active faults	Strike-Slip	Depleted Oil Field with Complex Stress History	Stiff rock/long term	-
0	No record	Few Reservoir Faults; Far from active faults	Normal	High Perm Large Aquifer/Depleted Gas Field	No cooling or soft reservoir	-
Max	2	2	2	2	2	14.0
Weight	1	1	1	3	1	
P18	0	1	0	0	1	0.14
In Salah	0	2	1	2	0	0.64
Sleipner	0	1	0	0	0	0.07
Weyburn	1	2	1	1	0	0.50

Risk Classification

Apart from compaction and injection, repressurization might also present a seismicity risk. After full depletion, the reservoir pressure will rise by 20bar per year during CO2 injection (TNO, 2019). This is similar to the refill of a gas storage like Bergermeer (Fenix, 2018), Grijpskerk or Norg. These gas storage reservoirs have induced some seismicity during refill, which could be explained in the case of Bergermeer from the earthquakes that occurred during depletion.
A review of seismic risk in gas storage reservoirs (Teatini *et al*., 2019) concluded that seismicity during refill is unlikely if no seismicity occurred during primary depletion. The guidelines for safe operation of gas storage reservoirs that never induced seismicity during depletion read:

> *"If no seismicity has been recorded during primary production, maximum reservoir pressure can safely be equal to initial pressure. Indeed, the system behaves elastically, and the pressure recovery unloads the faults to their initial criticality condition***.**
>
> *If no seismicity has been recorded during primary production and cushion gas injection, reservoir pressure change can safely span the whole pressure change between initial pressure and cushion gas pressure. As above, the system behaves elastically within the pressure range experienced by primary production and cushion gas injection. Therefore, a gas storage reservoir within the same range of pressure variation does not yield the system toward a more critical condition in terms of fault reactivation."*

It can be concluded that both with regard to compaction/repressurization seismicity and for injection seismicity, the P18 field falls in the class with negligible risk. Both the subsurface conditions indicate very low risk of fault slippage over a large area and the surface risk is also negligible since only a few nearby wellhead platforms are in the range of potential earthquake vibrations. Since the main concern with seismicity is not damage to surface structures, but CO2 migration due to fault slippage, it can be concluded that the low risk of seismicity results also in low risk of opening migration paths along the faults.

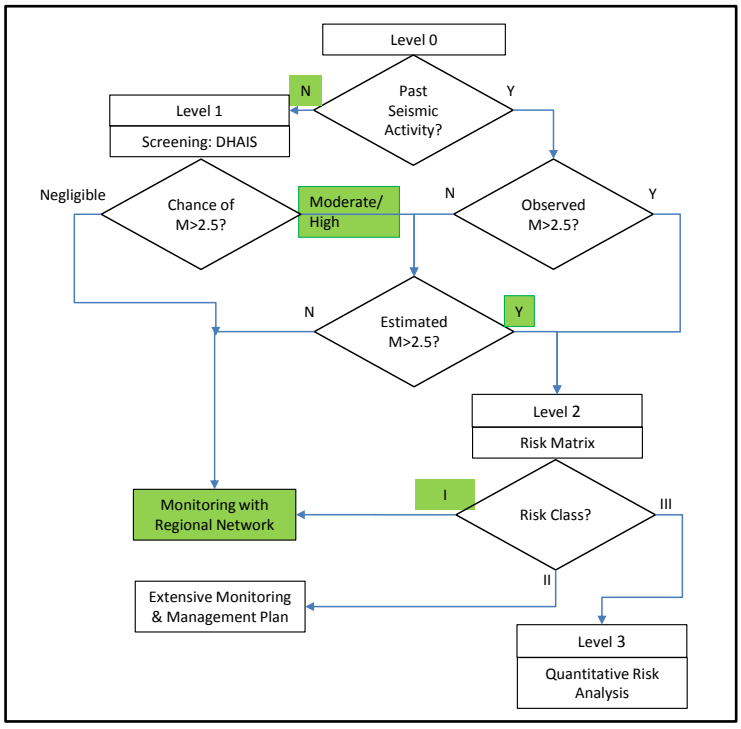

Figure 32: Decision flow diagram for Seismic Risk Classification proposed by SoDM. There has been no past seismicity in P18 and the risk matrices for compaction as well as injection risk yield risk class I of negligible risk, monitoring with the regional network is sufficient.

SoDM guidelines for seismic risk analysis outline a decision tree for determining the risk level, shown in Figure 32. Since P18 and neighbouring fields have no history of induced seismicity due to compaction and the risk of injection seismicity is very low, the decision tree yields standard monitoring with the regional network as the appropriate action.

Discussion

The hazard presented by potential fault slippage is deemed to yield a negligible risk, since seismicity is very unlikely in the P18 field. The guidelines for estimating maximum magnitude of seismicity yield a high value of moment magnitude M=4 for potential earthquakes. However, this is only a possibility if an entire fault would slip. In view of the historical depletion behavior, a realistic estimate of maximum magnitude is M=2 because no seismicity has been observed with the regional monitoring system, while sections along the faults are critically stressed by compaction (TNO, 2019). The injection of CO2 will raise the pressure, which will stabilize the faults. Any injection seismicity is only observed when faults were already active during depletion, while non-seismic reservoir will also be non-seismic during re-pressurization (Teatini *et al*., 2019). So, we cannot rule out that the P18 field has fault sections that are critically stressed so that they induce weak earthquakes that have gone undetected. Such weak earthquakes correspond with rather small slippage area. It is not expected that pressure increase will create larger critically stressed fault areas that could induce larger earthquakes.
The absence of seismicity in P18 is likely related to the absence of seismicity in the entire area, which has many producing gas fields. For instance, the Monster field has been fully depleted without inducing seismicity. As yet, the non-seismic character of the faults in the P18 area cannot be explained. It is remarkable that also other areas in the Netherlands show no seismicity while the gas fields in those areas have been fully depleted and also other reservoir properties are similar to gas fields that have induced seismicity (Vörös et al., 2019). Actually, the compaction seismicity is concentrated in two clusters, while gas fields outside these clusters appear to be non-seismic.
Future seismicity cannot be ruled out, because some small faults may still be stressed by cooling of the reservoir. However, any seismic slippage will be confined to the fault area in the vicinity of the reservoir, because only the fault height close to the reservoir will become critically stressed. The seal layers overlying the reservoir are much thicker than the reservoir, so that there is negligible risk of ever breaching the seal by fault slippage, as also concluded in the study by TNO (2019).

References

Baisch, S., Koch, C., Stang, H., Pittens, B., Drijver, B., & Buik, N. (2016). Defining the framework for seismic hazard assessment in geothermal projects V0.1. Technical Report, Report No. 161005, Bad Bergzabern, Germany: prepared for KennisAgenda Aardwarmte.

Bois, A., Mohajerani, M., Dousi, N., & Harms, S. (2013). Inducing Earthquake by Injecting Water In A Gas Field: Water-weakening Effect. SPE Annual Technical Conference and Exhibition, 30 September - 2 October 2013, New Orleans, Louisiana, USA.

Committee on Induced Seismicity Potential in Energy Technologies. Induced Seismicity Potential in Energy Technologies. The National Academies Press (2013).

Davies, R., Foulger, G., Bindley, A., & Styles, P. (2013). Induced seismicity and hydraulic fracturing for the recovery of hydrocarbons. Marine and Petroleum Geology, 45 (0), 171-185.

Davis, S. D., & Frohlich, C. (1993). Did (or will) fluid injection cause earthquakes? - criteria for a rational assessment. Seismological Research Letters, 64 (3-4), 207-224.

De Crook, Th., H.W. Haak & B. Dost (1998). Seismich risico in Noord-Nederland.KNMI (Koninklijk Nederlands Meteorologisch Instituut), Techn. Rep., De Bilt, Netherlands.

Deichmann, N., Kraft, T., & Evans, K. F. (2014). Identification of faults activated during the stimulation of the Basel geothermal project from cluster analysis and focal mechanisms of the larger magnitude events. Geothermics, 52 , 84-97.

Dost, B., Goutbeek, F., van Eck, T., Kraaijpoel, D. (2012) Monitoring induced seismicity in the North of the Netherlands: status report 2010. WR 2012-03.

Dost, Bernard et al., 2012. Monitoring induced seismicity in the North of the Netherlands: status report 2010,

Dowrick, David J. and David A. Rhoades, (2004), "Relations Between Earthquake Magnitude and Fault Rupture Dimensions: How Regionally Variable Are They?", Bulletin of the Seismological Society of America, Vol. 94, No. 3, pp. 776–788, June 2004.

English, J.M., (2012), "Thermomechanical origin of regional fracture systems", AAPG Bulletin, v. 96, no. 9 (September 2012), pp. 1597–1625.

Fenix Consulting Delft BV (Febr.2016)," Geomechanical Support for BGS+ Storage Plan Permit Application", Report for TAQA Energy BV.

Foulger, G. R., Wilson, M. P., Gluyas, J. G., Julian, B. R., & Davies, R. J. (2018). Global review of human-induced earthquakes. Earth-Science Reviews, 178 , 438-514.

Geertsma, J. and van Opstal, G. (1973). A Numerical Technique for Predicting Subsidence Above Compacting Reservoirs, Based on the Nucleus of Strain Concept. Verh. Kon. Ned. Geol. Mijnbouwk. Gen., 28, pp. 63-78.

Grigoli, F., Cesca, S., Rinaldi, A. P., Manconi, A., López-Comino, J. A., Clinton, J. F., Westaway, R., Cauzzi, C., Dahm, T., & Wiemer, S. (2018). The November 2017 Mw 5.5 Pohang earthquake: A possible case of induced seismicity in South Korea. Science, 360 (6392), 1003-1006.

Hagoort, J.J. (1980), "Modeling the Propagation of Waterflood-Induced Hydraulic Fractures", SPE-7412-PA.

Hangx , S.J.T., C.J. Spiers, C.J. Peach, A. ten Hove and A.M.H. Pluymakers, "Mechanical behaviour and transport properties of anhydrite - implications for caprock integrity during long-term storage of CO2", Geophysical Research Abstracts, Vol. 14, EGU2012-9379-1, 2012.

Heap, M.J., M. Villeneuve, A.R.L. Kushnir, J. Farquharson, P. Bauda, T.Reuschlé , (2019), "Rock mass strength and elastic modulus of the Buntsandstein: An important lithostratigraphic unit for geothermal exploitation in the Upper Rhine Graben", Geothermics, Volume 77, January 2019, Pages 236-256

Houtgast, G. Aardbevingen in Nederland. KNMI report 179. KNMI, de Bilt (1992).

Kanamori, H. (1994), Mechanics of Earthquakes. Annual Rev. Earth Planet Sci., 22, p207-237.

Kim, K., Ree, J., Kim, Y., Kim, S., Kang, S. Y., & Seo, W. (2018). Assessing whether the 2017 Mw 5.4 Pohang earthquake in South Korea was an induced event. Science (New York, N.Y.), 360 (6392), 1007.

KNMI, Bernard Dost, Femke Goutbeek, Torild van Eck and Dirk Kraaijpoel, (2010), "Monitoring induced seismicity in the North of the Netherlands: status report 2010"", De Bilt, 2012 | Scientific report; WR 2012-03.

Koning, E.J.L. (1988), "Waterflooding under fracturing conditions", PhD thesis TU Delft.

Kraaijpoel, D. et al., 2008. Location of induced earthquakes in the Netherlands gas fields. In ESC General Assembly 2008, September 7-12, 2008, Hersonissos.

Logan, J.M., C.A. Dengo, N.G. Higgs, Z.Z. Wang, (1992), "Fabrics of experimental fault zones: their development and relationship to mechanical behaviour", in Fault Mechanics and Transport properties of rock, ed. Evans, Wong), Academic Press.

McGarr, A., 1976. Seismic Moments and Volume Changes. Journal of Geophysical Research, 81(8), pp.1487–1494.

NAM, (2013), "Winningsplan Monster Field", NLOG_FieldAsset_8243_wipla_Gaag_Monster_PUB.pdf on http://www.NLOG.nl.

Nicholson, C., R.L. Wesson, (1990), "Earthquake hazard associated with deep well injection- A report to the US Environmental Protection Agency", USGS 1951, Appendix A, p65.

Pater, C.J. de and S. Baisch, 2011. Geomechanical Study of Bowland Shale Seismicity. Synthesis Report prepared for Cuadrilla Resources Ltd., 71 pages.

Roest, J.P.A., Kuilman, W. (1993). Geomechanische Analyse van de lichte aardschokken in het Eleveld reservoir, TU-Delft.

Roest, J.P.A., Kuilman, W. (1994). Geomechanical analysis of small earthquakes at the Eleveld gas reservoir. In: 'Eurock '94; SPE/ISRM international conference, Delft, Netherlands', pp. 573–580.

Rutledge, James, Xiaowei Weng, Chris Chapman, Xin Yu, and Scott Leaney, (2015), "Bedding-plane slip as a microseismic source during hydraulic fracturing", p926, THE LEADING EDGE, August 2015.

Scholz, Christopher H. Earthquakes and friction laws. Nature (1998) 391(1st January 1998): 37-42.

Segall, P., & Lu, S. (2015). Injection-induced seismicity: Poroelastic and earthquake nucleation effects. Journal of Geophysical Research: Solid Earth, 120 (7), 5082-5103.

STAATSTOEZICHT OP DE MIJNEN, (2016), "METHODIEK VOOR RISICOANALYSE OMTRENT GEÏNDUCEERDE BEVINGEN DOOR GASWINNING TIJDELIJKE LEIDRAAD VOOR ADRESSERING MBB. 24.1.P, VERSIE 1.2", Den Haag

Teatini, P., C. Zoccarato, M. Ferronato, A. Franceschini, G. Isotton, M. Frigo, C. Janna, (2019), "KEM-01 Geomechanical factors determining fault criticality during pressure cycling of underground gas storage in (see.

Thienen-Visser, L van, M. Nepveu, J. Hettelaar "Deterministische hazard analyse voor geïnduceerde seismiciteit in Nederland", TNO 2012 R10198, (2012),

TNO (2015), "Quick scan of Induced Seismicity Potential for small onshore depleting gas fields in The Netherlands", 2015 R10295.

TNO (2018), "Inventarisatie aantoonbare effecten voor mens en milieu als gevolg van historische conventionele frackoperaties", TNO2018 R10807 -Eindrapport, 11 september 2018.

TNO, (2019), "CO2 storage feasibility in the P18-2 depleted gas field", August 2019, TNO report 11111, Authors: Neele, F, T. Wildenborg, K. Geel, D. Loeve, L. Peters, S. Kahrobaei, T. Candela, M. Koenen, P.Hopmans, K. van der Valk, B. Orlic, V. Vandeweijer.

Vörös, R., S. Baisch, (2019), "Geomechanical Study – Small Gas Fields in the Netherlands", State Supervision of Mines (SodM), KEM program report, Version 1, Archive No.: SODM002.